Chemical Engineering Journal 155 (2009) 272–284

Contents lists available at ScienceDirect

Chemical Engineering Journal

journal homepage: www.elsevier.com/locate/cej

Theoretical modelling of the effect of surface active species on the mass transfer rates in bubble column reactors

Mariano Martín[a,b,*], Francisco J. Montes[b], Miguel A. Galán[b]

[a] Chemical Engineering Department, Carnegie Mellon University 5000 Forbes Avd, Pittsburgh, PA 15213, USA
[b] Departamento de Ingeniería Química y Textil, Universidad de Salamanca Pza, de los Caídos 1-5, 37008 Salamanca, Spain

ARTICLE INFO

Article history:
Received 5 May 2009
Received in revised form 10 August 2009
Accepted 11 August 2009

Keywords:
Population balance
Mass transfer
Bubble columns
Contaminants
Surface tension
Mathematical modelling

ABSTRACT

The complex composition of the liquid media in bubble column reactors makes their understanding and theoretical modelling challenging. In this work we have studied the effect of surface tension and contaminants, salts, on the mass transfer rates from a theoretical point of view, looking for a deeper understanding on the effect of surface active species which usually reduce surface tension and modify bubble surface behaviour. The specific contact area is obtained using a population balance where the effect of the presence of contaminants is addressed by the proper theoretical closures for bubble coalescence efficiency, for partially and fully immobile surfaces, and bubble break-up. Meanwhile, the contribution of contaminants to the liquid-film resistance is implemented as function of the coverage of the surface of the bubbles. It was found that the degree of bubble surface coverage not only affects bubble coalescence but also their break-up. The ion strength defines bubbles stability and the critical Weber number can be predicted as function of ion strength. Furthermore, the mass transfer rates are function of the surface coverage by the electrolytes. The model was able to predict k_La taking into account the fact that the concentration profiles surrounding individual bubbles are not completely developed due to the presence of other bubbles, in agreement with previous results from the literature.

1. Introduction

Bubble column reactors (BCR's) are widely used in the chemical and biochemical industries because of the advantages they offer in terms of gas–liquid contact area and mass/heat transfer rates [1–3]. For processes sensible to shear stress, like those involving cell cultures, BCR's are the most suitable solutions [4,5]. However, the problem of supplying adequate oxygen to the liquid phase inside arises because of the limited solubility of this element in water and water solutions. Thus, the mass transfer rates become the limiting stage [6].

Therefore, the most important parameter affecting the design, scale-up and operation of bubble columns is the volumetric mass transfer coefficient, k_La. The later is function of the contact area between the gas phase and the liquid phase, "a", and the resistance to mass transport in the liquid side, k_L. In order to predict k_La the influences of the different processes and mechanisms affecting both variables must be addressed.

Over the years, the design of bubble columns and the prediction of k_La has been addressed either using empirical correlations based on dimensionless numbers [1,7,8] or using different theoretical or semi-theoretical approaches like Kawase et al.'s [9] or Shimizu et al.'s models [10], Computational Fluid Dynamics (CFD) simulations [11], the use of Continuous Stirred Tank Reactor (CSTR) and Axial Dispersion Models (ADM) or its derivatives, slug and cell models [12–15], or neural networks [16]. Good theoretical models are necessary to obtain better understanding of the phenomena taking place inside bubble columns. However, most of the theoretical models focus on the air–water system and/or rely on a number of adjustable parameters regarding the population balances and the mass transfer rates.

The physical properties of culture broths are far more complex than the air–water system. A typical fermentation medium is comprised of many species like different salts, hydrocarbons, alcohols, organic nutrients, surfactants, ... [17–21], etc., providing a wide range of physical properties to the liquid phase which affect not only the mechanisms of the physical processes involving bubbles, namely bubble formation, coalescence and break-up, but also the mass transfer rates.

The effect of liquid viscosity has been theoretically addressed in a previous paper [22]. According to that work, liquid viscosity attenuates the concentration gradients surrounding the bubbles by means of absorbing bubble oscillations reducing "k_L". Bubbles are

* Corresponding author at: Departamento de Ingeniería Química y Textil, Universidad de Salamanca Pza, de los Caídos 1-5, 37008 Salamanca, Spain.
Tel.: +34 923294479; fax: +34 923294574.
E-mail address: mariano.m3@usal.es (M. Martín).

1385-8947/$ – see front matter © 2009 Elsevier B.V. All rights reserved.
doi:10.1016/j.cej.2009.08.009

Nomenclature

a	specific contact area (m^{-1})
B_i	break-up frequency ($m^{-3}\,s^{-1}$)
clearance	distance between the perforated area and the column diameter (m)
C_{ij}	coalescence frequency for bubbles of classes i,j ($m^{-3}\,s^{-1}$)
d_b	bubble diameter (m)
db_{ini}	bubble diameter at the orifice (m)
d_e	diameter of the eddies (m)
d_{eq}	equivalent diameter of the bubbles (m)
d_{ij}	diameter of the bubble resulting from coalescence of two (m) defined by Eq. (19)
D_C	column diameter (m)
d_o	orifice diameter (m)
$D_L = D_{air-water}$	air diffusivity in water ($m^2\,s^{-1}$)
Eo	Eötvös number $Eo = (\rho_L - \rho_G)\cdot g \cdot d_{eq}^2/\sigma$
e_i	eccentricity. Defined by Eq. (51)
F	force applied between bubbles (N)
f_ε	correction factor for the gas hold up as function of the ionic force
f_{k_La}	correction factor for the volumetric mass transfer coefficient as function of the ionic force
f_{db}	correction factor for the bubble mean size as function of the ionic force
g	acceleration due to gravity ($m\,s^{-2}$)
G	generation function defined by Eq. (35)
h_0	initial thickness of the drainage film (m)
h_f	final thickness of the drainage film (m)
I	ionic strength (M)
k	wave number $k = 2/d_e$ (m^{-1})
k_L	liquid-film resistance ($m\,s^{-1}$)
k_La	volumetric mass transfer coefficient (s^{-1})
M	Morton number $M = g\cdot\mu_L^4/\rho\cdot\sigma^3$
n_i	concentration of class i elements per unit volume (n^o bubbles m^{-3})
$n_{b,i}$	number of bubbles of class i (n^o bubbles)
n_e	concentration of eddies per unit volume (n^o bubbles m^{-3})
n_{2Gen}	bubbles of class 2 generated at the sparger (n^o bubbles $m^{-3}\,s^{-1}$)
$n_{orifices}$	actual number of orifices
N_o	number of orifices
N_{oa}	number of orifices per area (m^{-2})
N_e	eddies concentration (eddies kg^{-1} liquid)
P	hole pitch (m)
P_d	formation period of bubbles (s)
Q_c	gas flow rate ($m^3\,s^{-1}$)
r	bubble radius (m)
r_C	column radius (m)
$S_{b,i}$	surface contact area of the non-spherical bubble (m^2)
Se	fraction of the bubble surface covered by contaminants
S_{ij}	surface contact area (m^2)
t	time (s)
t_{ij}	film drainage time (s)
u	generic length units
u_c	critical velocity of a bubble ($m\,s^{-1}$)
u_r	rising velocity of a bubble ($m\,s^{-1}$)
u_t	turbulent velocity ($m\,s^{-1}$)
U_l	liquid velocity ($m\,s^{-1}$)
u_G	superficial gas velocity ($m\,s^{-1}$)
V_b	bubble volume (m^3)
V_s	liquid volume in the column (m^3)
We	Weber number: $We = d_{eq}\cdot u_r^2\cdot\rho_L/\sigma$
x_j	fraction of bubble of class j
z	vertical coordinate (m)

Greek symbols

κ	break-up efficiency
ε	dissipated turbulent energy ($W\,kg^{-1}$)
ε_g	gas hold-up
λ_{ij}	collision efficiency
θ_{ij}	collision frequency ($m^{-3}\,s^{-1}$)
μ_L	liquid viscosity (Pa s)
μ_G	gas viscosity (Pa s)
ν_L	kinematic viscosity of the liquid ($m^2\,s^{-1}$)
ρ_L	liquid density ($kg\,m^{-3}$)
ρ_G	gas density ($kg\,m^{-3}$)
σ	surface tension ($N\,m^{-1}$)
τ_{ij}	contact time between bubbles (s)
μ_{dist}	mean value of the distribution
σ_{dist}	standard deviation

Superscripts

Mobile	part of the bubble that behaves as a mobile surface
Solid	part of the bubble that behaves as a rigid surface
T	turbulent
B	buoyancy
LS	laminar stress

also more stable in viscous liquids since bubble deformation and break-up is diminished resulting in bigger bubbles and determining the contact area "a". The authors found that the critical Weber number, We_c, controls bubble break-up and We_c was successfully correlated as function of the liquid viscosity.

Many bioprocesses need surface active species like salts [17,19,20] and different types of surfactants/alcohols are also often produced [18,23]. Salts together with surfactants affect bubble surface properties. These species gather themselves in the surface of the bubbles and modify the movement of the liquid layers surrounding the bubbles, which results in determining the gas–liquid contact area and the mass transfer mechanisms. Some research groups have focused on evaluating the effect of the presence of different salts and surface active agents on the liquid-film resistance experimentally [24–36] and some theoretical models have been proposed [37,38]. However, when it comes to the contact area, its modelling is empirical [26,31,34,36,39] or a number of parameters must be used for each particular case [39,40].

Thus, this paper addresses the problem of theoretically predicting the effect of surface active species (salts, alcohols, surfactants, etc.) on the mass transfer rates by means of predicting k_La in the homogenous regime, preferable for applications involving sensitive materials like bioreactors, blood oxygenators where oxygen transfer is limiting for the process and the effect of surface active species is also common. Surface active species show two effects: first, they reduce the surface tension and second, they modify the properties of the bubble surfaces. In order to get better understanding we have broken down both effects studying the contribution of surface tension and that of salts on k_La in bubble columns, extending previous works by the authors [22,41] and the literature [1,7,8,34,37,38]. The model couples a population balance model (PBM) with a model for the liquid-film resistance. It accounts for the effect of contaminants on bubble coalescence and break-up using theoretical closures which assume that the presence of surface active species

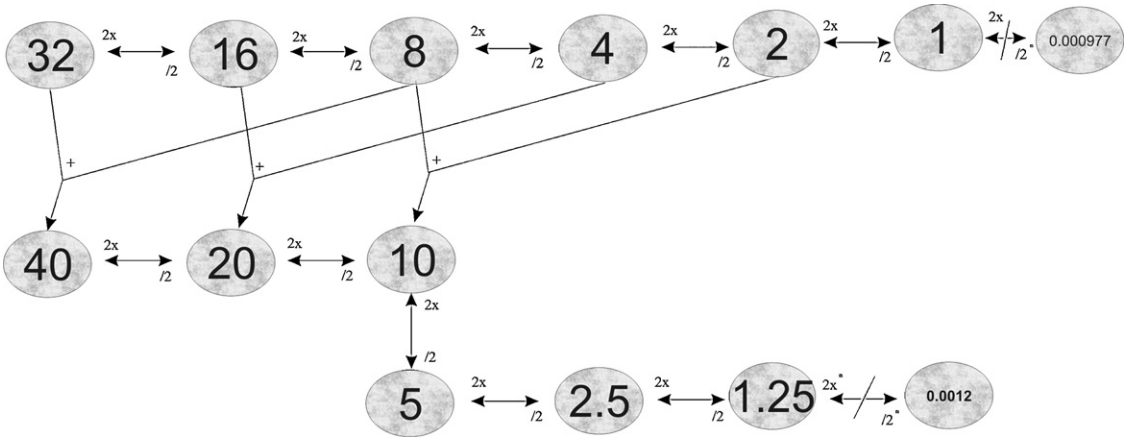

Fig. 1. Scheme of bubbles present in the column.

reduce the mobility of the liquid layers surrounding the bubbles affecting bubble rise velocities, the liquid drainage, bubble stability, mass transfer resistances, etc. The use of theoretical closures attempts to give physical meaning and understanding to the number of adjustable parameters used so far by CFD commercial codes [39,40]. The bubbles are assumed to be non-spherical to improve the determination of the specific contact area [41–43]. Experimental results for Sauter-mean bubble diameter, d_{32}, and k_La from the literature [1,7,8,34] have been used to validate the model proposed.

2. Theoretical model

A small amount of surface active component has the effect of retarding the coalescence of gas bubbles and, thus, makes the gas–liquid interfacial area larger. It also has the effect of resisting the stretching and compression of the interface, therefore reducing the disturbance in the bulk fluids, and making the resistance to mass transfer larger and consequently the mass transfer coefficient smaller [44]. Because of these two opposing factors, it is important to obtain a better understanding of the phenomenon to optimize the performance of BCR's. Therefore, the present model will determine the contact area provided by the bubbles using a PBM taking into account the effect of contaminants on bubble coalescence and break-up. The calculated specific contact area will be combined with the value for the liquid-film resistance, k_L, calculated as function of the surface coverage of the bubbles which determines the behaviour of their surfaces as mobiles or rigids.

2.1. Hydrodynamics

Fluid hydrodynamics involves the processes related to bubble formation, rising, coalescence and break-up. Bubble formation at the orifice will be the starting point to determine the dispersion of bubbles. Then, different closures for the efficiency of bubble coalescence and break-up will be used depending on the degree of contamination of the bubble surfaces [45–47].

2.1.1. Bubble scheme

Bubble shape plays an important role on mass transfer mechanisms as it has been explained in the literature [22,41–43]. Therefore, in this paper we have implemented a scheme of bubbles, see Fig. 1 proposed in previous papers by the authors [22,41] so that the bubbles resulting from coalescence and break-up processes exist, accounting for the effect of bubble shape on the contact area. This scheme also avoids problems regarding the total gas phase in the tank.

For the sake of simplicity numbers are given to represent the relative volume of the bubbles present in the bubble column, Fig. 1. We consider that the initial bubble size at the sparger, which actually depends on the orifice diameter and the gas flow across, has a relative volume of $16u^3$.

(a) The diameter of the orifices of the sparger will be 0.005 m, which is preferred in industry [48].

(b) Bubble size at the orifice will be calculated in a simple way since the effect of the dispersion device is limited to very small bubbles and/or low energy dissipated ones [1,41]. For the experimental conditions considered let's assume Miller's ratio [49], Eq. (1), even though it is widely know that surface tension and surfactants affect bubble formation [31,50,51]. Both effects can be easily implemented in this framework if necessary.

$$db_{ini} = 3.5 \cdot d_o \tag{1}$$

(c) The configuration of the sieve plate is based on holes placed on 60° equilateral triangular pitch with the liquid flowing normally [52]. The recommended spacing to avoid unstable operation is from $2.5d_o$ to $5d_o$. In this paper $3.5d_o$ will be used [2,49]. According to this typical configuration the number of orifices in a sieve plate is given by Ludwig [52]:

$$N_{oa} = 1.158 \cdot \left(\frac{P}{0.0254}\right)^{-2}; \tag{2}$$

$$N_o = N_{oa} \cdot \left(\pi\left(\frac{D_c - \text{clearance}}{2}\right)^2\right); \tag{3}$$

Clearance will be 5% of D_c (D_c = 1 m)

From the initial bubble size at the orifice (relative volume of $16u^3$ in Fig. 1), bubble coalescence and break-up processes are allowed subjected to certain conditions to obtain different bubble classes/sizes. The relative bubble sizes in the column are represented in Fig. 1. The processes allowed (coalescence and break-up) are represented as arrows linking the bubbles sizes, circles, under consideration for each single process, with the operators used attached to the tip of the arrow defining the process ((2×) to identify that two bubbles of the same size merge to obtain another of the bigger volume, (/2) to talk about binary break-up of the bubbles into two equal ones or an operator (+) is located to say that those two bubbles of different size will coalesce).

Only binary break-up into two daughter bubbles is considered for all bubble sizes, since it is overwhelmingly the major break-up manner supported by experimental observations [53–55] Furthermore, it will be assumed that a bubble breaks into two equal size

daughter bubbles, which has proved to be successful in modelling the hydrodynamics of bubble columns [10,56] and stirred tanks [57]. Eq. (4) allows determining the volume of the bubbles generated in the break-up. Thus, the volume of the bubbles is calculated as follows:

$$2 \cdot \frac{4}{3}\pi\left(\frac{d_{b,j+1}}{2}\right)^3 = 2 \cdot V_{b,j+1} = V_{b,j} = \frac{4}{3}\pi\left(\frac{d_{b,j}}{2}\right)^3 \quad (4)$$

According to Fig. 1, bubbles of relative volumes of 1 and 1.25 (see Fig. 1) can be broken up to 10 times more. These simplifications will allow handling the effect of bubble break-up in generation of area and the effect of bubble shape on the mass transfer, while maintaining the total gas phase monitored.

In order to simulate bubble break-up and coalescence, we are going to introduce the closures used in this model.

2.1.2. Bubble coalescence

Coalescence is has two effects on the mass transfer rates: (a) coalescence decreases the specific contact area and (b) its effect on the bubble shape and deformation leads to an enhancement in mass transfer rates as a result of the oscillations derived from the process of coalescence itself [41,58]. The presence of contaminants adds complexity to the process in pure liquids [47,59–70]. In the presence of contaminants like electrolytes or surfactants, the bubble surfaces are modified reducing the film drainage. Moreover, the concept of a transition concentration, above which bubble coalescence is drastically reduced, is already well established in the literature [71–74] and becomes key when modelling the effect of the salts or surfactants on the bubble size distribution in gas–liquid equipment.

The model for bubble coalescence is based on the study of bubble collisions. Different mechanisms are responsible for bubble collision. However, not every collision leads to coalescence. Thus, Prince and Blanch [45] proposed a model for bubble coalescence in bubble columns where the coalescence rate, C_{ij} ($m^{-3}\ s^{-1}$), for two bubbles i, j whether they are of the same class ($i = j$) or not ($i \neq j$), is given by the product between the collision frequency and the efficiency by which that collisions derive in coalescence Eq. (5)

$$C_{ij} = (\theta_{ij}^{T} + \theta_{ij}^{B} + \theta_{ij}^{LS}) \cdot \lambda_{ij} \quad (5)$$

The equations for the different collision mechanisms for pure liquids can be found in Table 1 [41,45,56]. However, contaminated water as well as electrolytic solutions shows a reduction in the terminal rise velocity of the bubbles [76–80]. The theoretical equation for the terminal velocity of contaminated solutions is given by Grace et al. [80]

$$u_{ri} = \left(\frac{\mu_L}{d_{b,i} \cdot \rho_L}\right) \cdot J - 0.857 \cdot M^{-0.149} \quad (13)$$

where M is the Morton number and J is defined by Eq. (14)

$$J = \begin{cases} 0.94 \cdot N^{0.757} & 2 < N \leq 59.3 \\ 3.42 \cdot N^{0.441} & N > 59.3 \end{cases} \quad (14)$$

where N is given by Eq. (15)

$$N = \frac{4}{3} Eo \cdot M^{-0.144}\left(\frac{\mu_L}{0.0009}\right)^{-0.14} \quad (15)$$

Not every collision results in coalescence. Coalescence probability depends on the intrinsic contact between bubbles. Coulaloglou and Tavlarides [82] defined the collision efficiency between bubbles of classes i and j, λ_{ij}, as a probability function given by Eq. (16) which depends on the relationship between the time required for film drainage, t_{ij}, and the contact time of the bubbles, τ_{ij}. Table 2 summarizes the equations for collision efficiency for pure liquids.

In case the liquid contains surface active species (ions, alcohols, surfactants, contaminants, etc.), the structure of the water changes, affecting bubble coalescence. The presence of salts or surfactants modifies the drainage of the liquid between two colliding bubbles by means of transforming the bubble surface from mobile to immobile. Structure builders bring about strong electric fields, which not only polarize, immobilize and electrically strengthen the neighboring water molecules, but also cause additional ordering (entropy loss). The substance which reduced the solution entropy the most also inhibited the coalescence at the lowest concentration. For the same charge, the size of the species also determines the effect upon coalescence. Smaller ions exerted a larger effect on the water molecules because they produce a higher charge density [44]. Surface tension and bubble surface contamination can also be affected by the size of the ions and further experimental data are needed. For more information see supplementary material.

Depending of the concentration of contaminants (salts, surfactants, etc.), the surfaces will be partially mobile or fully immobile. The concept of critical concentration is thus key to determine this limit. The actual value of concentration depends on the species but has already been studied in the literature [71–74]. Until the critical concentration is reached, the bubble surfaces will behave as par-

Table 1
Basic model for the collision frequency in a bubble column.

Collision mechanism	Contact area	Collision velocity
$\theta_{ij}^{T} = n_i \cdot n_j \cdot S_{ij} \cdot (u_{ti}^2 + u_{tj}^2)^{0.5}$ (6)	$S_{ij} = \frac{\pi}{16}(d_{bi} + d_{bj})^2$ (7)	$u_t = 1.4 \cdot \varepsilon^{1/3} \cdot d_b^{1/3}$ [75] (8)
$\theta_{ij}^{B} = n_i \cdot n_j \cdot S_{ij} \cdot (u_{ri} - u_{rj})$ (9)		$u_{ri} = \left(2.14 \cdot \frac{\sigma}{\rho_L \cdot d_{bi}} + 0.505 \cdot g \cdot d_{bi}\right)^{0.5}$ (10)
$\theta_{ij}^{LS} = n_i n_j \cdot \frac{4}{3} \cdot \left(\frac{d_{bi}}{2} + \frac{d_{bj}}{2}\right)^3 \cdot \left(\frac{dU_1}{dr}\right)$ [81] (11)		$\left(\frac{dU_1}{dr_C}\right) \approx \frac{U_1}{D_C/2} = \frac{0.787(g \cdot D_C u_G)^{1/3}}{D_C/2}$ (12)

D_C is the diameter of the BCR. We are going to consider D_C to be equal to 1 m.

Table 2
Coalescence efficiency in pure liquids.

Break-up efficiency	Contact time [45]	Drainage time [45,83]
$\lambda_{ij} = \exp\left(-\frac{t_{ij}}{\tau_{ij}}\right)$ (16)	$\tau_{ij} = \frac{(0.5 \cdot d_b)^{2/3}}{\varepsilon^{1/3}}$ (17)	$t_{ij} = \left(\frac{(0.5 \cdot d_{ij})^3 \cdot \rho_L}{16 \cdot \sigma}\right)^{0.5} \ln\left(\frac{h_0}{h_f}\right)$ (18)
		$d_{ij} = \left(\frac{2}{d_{bi}} + \frac{2}{d_{bj}}\right)^{-1}$ (19)

tially mobile and thus the drainage time is modifies from Eqs. (18) to (20) [46]

$$t_{ij} = \left(\frac{\pi}{2} \frac{\mu_L(\rho_L \cdot (\varepsilon^{2/3}(d_i + d_j)^{2/3})^2)^{1/2} \left(d_i \cdot d_j / d_i + d_j\right)^4}{(2 \cdot \pi \cdot \sigma)^{3/2}} \right) \cdot \left(\frac{1}{h_f} - \frac{1}{h_0} \right) \quad (20)$$

Above the critical concentration, the whole bubble surface will be covered by the species modifying the behaviour of the surface to become immobile. Thus, Eq. (21) [46] will be applied

$$t_{ij} = \frac{3}{16} \left(\frac{\rho_L \cdot \varepsilon^{2/3} \cdot (d_i + d_j)^{2/3} (d_i \cdot d_j / d_i + d_j)^2 \mu_L}{\pi \cdot \sigma} \right) \cdot \left(\frac{d_i \cdot d_j}{d_i + d_j} \right)^2 \cdot \left(\frac{1}{h_f} - \frac{1}{h_0} \right) \quad (21)$$

In accordance with the results gathered by Prince and Blanch [45] we are going to consider:

$$h_0 = 1 \times 10^{-4}\,\text{m} \quad (22)$$

$$h_f = 1 \times 10^{-8}\,\text{m} \quad (23)$$

2.1.3. Bubble break-up

Bubbles in the flow inside BCR's are deformed and eventually break. Prince and Blanch [45] modelled bubble breakage as if the turbulent eddies collide with the bubbles deforming them and eventually breaking them. Therefore, the break-up rate is written as the product between the collision rate of bubbles and turbulent eddies and the efficiency of those collisions. Thus, the break-up frequency is:

$$B_i = \theta_{ie} \cdot \kappa_i \quad (24)$$

The collision velocity of turbulent eddies and bubbles is based on the same mechanism explained for bubble collision assuming that turbulent eddies behave as entities [45]. Table 3 summarizes the model.

The differential equation has to be solved using as lower and upper limits those given by Pohorecki et al. [56]. Only the eddies from $0.2d_b$ to d_b can actually break the bubbles. Smaller eddies do not have enough energy; meanwhile bigger ones drag the bubbles across the vessel [37]. Therefore, as a mean value, $d_e = 0.6d_b$ as has been proved valid for modelling bubble break-up [57].

Bubble break-up in bubble columns occurs when the liquid turbulence is high enough to deform the bubbles above their stable point, which depends on the physical properties of the liquid and on the fluid flow. Therefore, it is necessary to determine which eddies have enough energy to break the bubbles. Bubble break-up efficiency can be written as Eq. (31) [56]:

The critical Weber number (We_c) depends on the bubble break-up mechanism [57,84,85] and it is also function of the liquid viscosity because it stabilizes the bubbles [22]. The value originally used for modelling BCR's by Prince and Blanch [45] was 2.3. However, Shimizu et al. [10] used $We_c = 1$ in their model. Thus, it is expected that in presence of contaminants surrounding the bubble, its surface is modified determining the ultimate break-up of the bubbles. Thus, We_c will be the parameter of the population balance to account for bubble stability.

2.1.4. Energy dissipation

Energy in the tank is responsible for bubble collisions and deformation as well as for maintaining bubble oscillation. The dissipated energy can be defined by Eq. (33) used by Shimizu et al. [10] and Pohorecki et al. [56]:

$$\varepsilon = u_G \cdot g \quad (33)$$

2.1.5. Dispersion generated

A population balance based on that proposed by Fleischer et al. [86] will determine the fraction of bubbles of each size. In steady state the population balance in a bubble column becomes [56]:

$$0 = G(z, d_b, t) \quad (34)$$

where G represents a balance between the coalescence and break-up processes [56]. In our case the function G is as follows:

$$G_i = \frac{1}{2} \sum_{k=1}^{2} \sum_{l=1}^{2} C_{i,kl} - \sum_{j=1}^{2} C_{ij} + 2 \cdot B_{i-1} - B_i \quad (35)$$

Bubbles are periodically generated at the dispersion device (primary bubbles or bubbles of class 1), so that Eq. (35) must be completed by Eq. (36) when applied for this bubble class, to account for their presence in the tank due to the bubbling process. Eq. (36) is another source of bubbles of class 1 as well as coalescence or break-up and thus is a term to be added to the right-hand side of Eq. (35).

$$n_{2Gen} = \frac{n_{orifices}}{V_s \cdot P_d} \quad (36)$$

where V_s corresponds to the liquid volume of study and P_d is the formation period of the bubbles in each experimental condition.

Eq. (34) will be applied for 30 real bubble classes. So, the model consists of 30 equations like that given by Eq. (34) where the break-up and coalescence rates have been defined by the equations presented along the paper.

In order to solve the hydrodynamic model, the total number of bubbles in the column will be determined by the gas hold-up, ε_g. To reduce the error when comparing experimental and calculated k_La, it is interesting to use a correlation for ε_g determined for

Table 3
Bubble break-up closures.

Break-up rate				
$\theta_{ie} = n_i \cdot n_e \cdot S_{ie} \cdot (u_{ti}^2 + u_{te}^2)^{0.5}$	(25)	Contact area	$S_{ie} = \frac{\pi}{16}(d_{bi} + d_e)^2$	(26)
		Collision velocity	$u_{te} = 1.4 \leq \varepsilon^{1/3} \cdot d_e^{1/3}$	(27)
		Eddies size [56,103]	$d_e = \left(\frac{\nu_L^3}{\varepsilon}\right)^{0.25}$	(28)
			$n_e = N_e \cdot \rho_L$	(29)
		Eddies concentration [56]	$\frac{dN_e(k)}{dk} = 0.1 \cdot \frac{k^2}{\rho_L}$	(30)
Break-up efficiency				
$\kappa_i = \exp\left(-\frac{u_{ci}^2}{u_{te}^2}\right)$	(31)	Critical vortex velocity [45,56]	$u_{ci} = \left(\frac{We_c \cdot \sigma}{d_{bi} \cdot \rho_L}\right)^{0.5}$	(32)

the same experimental device and conditions as those used when determining k_La as well as valid for the experimental values used. For a complete theoretical model, theoretical equations for ε_g for pure liquids are available as presented in [41]. Meanwhile, in case of contaminated solutions, the model by Kulkarni et al. [87] could have been used.

Thus, the correlation proposed by Akita and Yoshida [88], Eq. (37), has been used to determine ε_g for non-electrolyte systems.

$$\frac{\varepsilon_g}{(1-\varepsilon_g)^4} = 0.2 \cdot \left(\frac{g \cdot D_c \cdot \rho_L}{\sigma}\right)^{1/8} \cdot \left(\frac{g \cdot D_c^2 \cdot \rho_L^2}{\mu_L^2}\right)^{1/12} \left(\frac{u_G}{\sqrt{D_c \cdot g}}\right) \quad (37)$$

Akita and Yoshida [7] also provide values for k_La, which are necessary for the validation of the model. In this way, no error related to the bubble dispersion generated can be considered since the model will simulate the hydrodynamics for which the k_La values have been measured.

Meanwhile, for electrolyte solutions the equation obtained by Hikita et al. [89] has been employed:

$$\varepsilon_g = 0.672 \cdot f_{\varepsilon_g} \cdot \left(\frac{u_G \cdot \mu_L}{\sigma}\right)^{0.578} \cdot \left(\frac{\mu_L^4 \cdot g}{\rho_L \sigma^3}\right)^{-0.131} \left(\frac{\rho_G}{\rho_L}\right)^{0.062} \left(\frac{\mu_G}{\mu_L}\right)^{0.107} \quad (38)$$

where

$$\begin{array}{l} \text{For } 0 < I < 1.0\,\text{g} - \text{ion/L} \\ f_{\varepsilon_g} = 10^{0.0414I} \\ \text{For } I > 1\,\text{g} - \text{ion/L} \\ f_{\varepsilon_g} = 1.1 \end{array} \quad (39)$$

Similarly, Hikita et al. [8] also presented correlations for k_La for the same electrolytic solutions.

The number of bubbles of each class is calculated as a fraction of the total gas phase in the bubble column:

$$n_{b,j} = \frac{3 \cdot \varepsilon_g \cdot D_c^2 \cdot (4 \cdot D_c + \text{Vol}_{gas}/(\pi(D_c/2)^2))}{2 \cdot d_{b,j}^3} \cdot x_j \quad (40)$$

The bubble fraction of class j, x_j, must be calculated. In order to do so, only the homogeneous regime is going to be considered. It has been proved that the experimental monomodal distributions of bubbles in stirred tanks and bubble columns can be adjusted to a log-normal distribution [45,56,57,90]. Therefore, a log-normal distribution for the bubbles in the column is considered whose parameters μ_{dist} and σ_{dist} will be found from minimizing Eq. (41):

$$\sum G = 0 \quad (41)$$

2.1.6. Experimental correlations used for model validation

The Sauter-mean diameter of non-electrolyte dispersion calculated using the model will be compared with the value obtained from the correlation given by Eq. (42) [88]:

$$d_{32} = 26 \cdot D_c \cdot \rho_L \cdot \left(\frac{g \cdot D_c^2 \cdot \rho_L}{\sigma}\right)^{-0.5} \cdot \left(\frac{g \cdot D_c^3}{(\mu_L/\sigma)^2}\right)^{-0.12} \cdot \left(\frac{u_G^2}{g \cdot D_c}\right)^{-0.06} \quad (42)$$

According to the literature [90] the bubble size distribution in the air–water system is similar to that obtained in air–electrolyte solutions but the bubble size is smaller due to the inhibition of coalescence. Zieminski and Whittemore [90] analyzed the effect of ion concentration on bubble size for different salts and a constant gas flow rate, to come up with a relationship between the decrease in bubble size and the ion strength. We are going to use a correction factor as function of the ionic strength based on Zieminski and Whittemore [90] results, similarly as Hikita et al. did [8,89] to correct k_La and ε_g due to the presence of salts [8,89], to adapt Eq. (42), using Eq. (43)

$$f_{db} = 0.2514 \cdot I\,(\text{mol/L})^{-0.349} \quad (43)$$

Thus the Sauter-mean bubble diameter in case of electrolyte solutions will be the product between Eqs. (42) and (43), where Eq. (42) provides the effect of the energy input in the column meanwhile Eq. (43) adds the effect of the inhibition of coalescence. The experimental results by Keitel and Onken, Ruen-ngam et al., Jamialahmadi and Müller-Steinhagen [78,91,92] support the fact that turbulent energy and ionic strength determine the bubble mean diameter.

2.2. Mass transfer

2.2.1. Effect of surfactants on the liquid-film resistance

Sada et al. [93] exposed that the presence of contaminants decreases k_La values. Alves's research group [28–30,37] developed a model that interprets the mass transfer from bubbles in terms of bubble contamination, where bubble surface behaviour ranges from mobile to rigid, as a result of the presence of salts or contaminants at the interface. For a mobile interface, the penetration of dissolved gas is slight and Higbie's theory is valid [94]

$$k_L^{mobile} = 1.13\sqrt{\frac{u_r}{d_b}}\,D_L^{1/2} \quad (44)$$

For a rigid interface, bubbles behave like solid spheres. The liquid-film resistance, k_L, is then theoretically obtained by the equation proposed by Frossling [95] from laminar boundary layer theory

$$k_L^{rigid} = 0.6\sqrt{\frac{u_r}{d_b}} \cdot D_L^{2/3} \cdot \nu_L^{-1/6} \quad (45)$$

Surface coverage is employed to calculate an averaged liquid-film resistance, so that the presence of contaminants can be taken into account. In the model developed by Sardeing et al. [96] the surface coverage, *Se*, is the weight between Higbie's and Frossling's models, Eq. (46)

$$k_L = Se \cdot k_L^{mobile} + (1 - Se) \cdot k_L^{rigid} \quad (46)$$

Se = 0 implies that bubbles are completely free of surfactants at the gas–liquid interface (i.e., pure water). On the other hand, *Se* = 1 is the corresponding value for a surfactant-saturated gas–liquid interface. *Se* values between 0 and 1 imply that the interface is partially occupied by surfactant molecules below the saturation concentration. *Se* is function of the contact area provided by the bubbles and the concentration of salt from pure liquid to the critical ones that changes the bubbles surface from mobile to rigid. This model predicts that the mass transfer rates between two limits, namely, k_L^{mobile}, the mass transfer coefficient for a free surface (*Se* = 0), and k_L^{rigid}, the mass transfer coefficient for a saturated surface (*Se* = 1). For more information see supplementary material.

Another important consideration was introduced by Koynov et al. [97]. They presented the fact that in bubble swarms, bubbles no longer traveled by themselves, but rather in liquid perturbed by the wakes of neighboring bubbles. In addition, the concentration of gas dissolved in the liquid around the bubble in a swarm no longer depended only on the mass transfer from the bubble itself, but also on the mass transfer from the other bubbles in the swarm. These two factors resulted in a decrease in the mass transfer coefficient of the bubble swarm compared with a single bubble. Therefore, it

is considered that k_L theoretically obtained for one single bubble cannot be used in a dispersion of bubbles because the presence of other bubbles does not allow the complete development of the velocity and concentration gradients surrounding a bubble. A correction factor is applied. The theoretical one reported by Lamont and Scott [98], 0.4, and previously verified [41] has been used.

Finally, in this model we do not implement the effect of bubble oscillations as in the previous ones [22,41]. The framework is already prepared but further research is needed to develop and verify a model for the contribution of bubble oscillations in case of immobile surfaces. The oscillations could clean partially those surfaces.

2.2.2. Volumetric mass transfer coefficient

The theoretical value is calculated by combining the averaged liquid-film resistance given by Eq. (46) with the specific area determined by the population balance:

$$k_L a = \sum_{i=1}^{30} k_{L,i} \cdot n_i \cdot S_{b,i} = \sum_{i=1}^{30} \sqrt{\frac{4D_L}{\pi}} \left(\frac{\varepsilon \rho}{\mu_L}\right)^{1/4} \cdot n_i \cdot S_{b,i} \quad (47)$$

There are many examples of the importance of bubble deformation in the mass transfer rates [42,43] which improved the prediction of the mass transfer rates in bubble column reactors by studying the contribution of bubble shape. Bubbles are subjected to stresses that deform them. Bubbles generated in electrolytic solutions of potassium chloride are ellipsoidal [78]. Therefore, the contact area of each bubble can be considered as that of spheroids. So far, in this paper we have been working with equivalent diameters for the bubbles defined as:

$$d_{b,i} = \sqrt[3]{l_i^2 \cdot h_i} \quad (48)$$

where l_i is the length of the bubble and h_i its height. The ratio between both can be defined according to Kulkarni et al. [99]

$$\frac{h_i}{l_i} = \frac{1}{1 + 0.163 \cdot Eo^{0.707}} \quad (49)$$

And the area of the bubble, $S_{b,i}$, is given by Nedeltchev et al. [43]

$$S_{b,i} = \pi \frac{l_i^2}{2} \left[1 + \left(\frac{h_i}{l_i}\right)^2 \frac{1}{2e_i} \ln \frac{(1+e_i)}{(1-e_i)}\right] \quad (50)$$

where the eccentricity of a particular class of bubbles i, e_i, is

$$e_i = \sqrt{1 - \left(\frac{h_i}{l_i}\right)^2} \quad (51)$$

2.2.3. Experimental correlations used for validating $k_L a$

Experimental results from the literature have been used to validate the model. For non-electrolyte systems, the correlation proposed by Akita and Yoshida [7] is used:

$$k_L a = 0.6 \cdot \frac{D_L}{D_c^2} \cdot \left(\frac{\mu_L}{D_L \cdot \rho_L}\right)^{0.5} \left(\frac{D_c \cdot g \cdot \rho_L}{\sigma}\right)^{0.62} \left(\frac{D_c^2 \cdot g}{(\mu_L/\rho_L)^2}\right)^{0.31} \varepsilon_g^{1.1} \quad (52)$$

where ε_g is given by Eq. (37)

Meanwhile for electrolyte solutions Eq. (53) will be applied [8]:

$$k_L a = 14.9 \cdot f_{k_L a} \cdot \left(\frac{u_G \cdot \mu_L}{\sigma}\right)^{1.76} \left(\frac{g \cdot \mu_L^4}{\rho_L \cdot \sigma^3}\right)^{-0.248} \left(\frac{\mu_G}{\mu_L}\right)^{0.243} \left(\frac{\mu_L}{D_L \cdot \rho_L}\right)^{-0.604} \left(\frac{g}{u_G}\right) \quad (53)$$

where

$$\begin{aligned} &\text{For } 0 < I < 1.0\,\text{g} - \text{ion/L} \\ &f_{k_L a} = 10^{0.068I} \\ &\text{For } I > 1\,\text{g} - \text{ion/L} \\ &f_{k_L a} = 1.114 \times 10^{0.021I} \end{aligned} \quad (54)$$

At this point we acknowledge that the model is being tested for operating conditions in the homogeneous regime working at atmospheric pressure and temperature. In case of industrial operation for certain processes, elevated pressure and temperature are used. Under those conditions, other the model must be corrected to account for these effects.

3. Model verification procedure

Even the presence of small amounts of different species modifies the physical properties of the liquids. Once the effect of liquid viscosity has been studied [22] the effect of surface tension and surface active species is key to get a deeper understanding of the mass transfer mechanisms in fermentation media.

The presence of surfactants or surface active species in a liquid dispersion modifies not only the physical properties, usually showing a decrease in the surface tension (accompanied by a modification in the liquid density and viscosity), but also changes the behaviour of the bubble surfaces by covering the bubbles. Therefore, it is important to separate both effects to study them. These effects translate into the modification of contact areas and the liquid-film resistance; both effects will be broken down to study them as separately as possible.

In order to evaluate the effect of surface tension, the model will be evaluated to determine the contribution of surface tension (and density) on the bubble size and the mass transfer rates. Due to the difficulty in finding a number of fluids whose physical properties are similar but differ in their surface tensions, virtual solutions with surface tensions of 35, 45 and 60 mN/m will be evaluated maintaining constant the liquid density 1000 kg/m^3 and viscosity 0.001 Pa s. Later two more virtual solutions will be tested by keeping the surface tension an liquid viscosity fixed to 72 mN/m and 0.001 Pa s and using liquid density of 750 and 1250 kg/m^3 to discard the effect of liquid density on the We_c in bubble break-up. Table 4 summarizes the properties of these five virtual solutions. The basic experiment correspond to that of the air–water system (ρ_L = 1000 kg/m^3, σ = 72 mN/m, μ_L = 0.001 Pa s) and has already been evaluated in a previous study by the authors [41]. According to that study, the We_c turned out to be 5.

Once the parameters of the model have been evaluated, the experimental values for a pure liquid phase, cyclohexane [34] with physical properties ρ_L = 778 kg/m^3, σ = 24.8 mN/m and μ_L = 0.977 Pa s, $D_L = 3.27 \times 10^{-9}$ m^2/s, will be modelled as a validation for the effect of surface tension and liquid density on the critical Weber number.

Due to the fact that surfactants not only reduce the surface tension but also modify the behaviour of the liquid layers surrounding the gas bubbles, in a second stage, the contribution of contaminants will be studied to evaluate the effect of impurities in bubble size

Table 4
Properties of the virtual solutions used.

Solution	Density (kg/m^3)	Surface tension (mN/m)	Viscosity (Pa s)
I	1000	0.030	0.001
II	1000	0.045	0.001
III	1000	0.060	0.001
IV	750	0.072	0.001
V	1250	0.072	0.001

Table 5
Properties of the electrolyte solutions used.

Solution	Concentration (M)	Density (kg/m^3)	Surface tension (mN/m)	Viscosity (Pa s)
A	0.01	1000	0.0710	0.001
B	0.02	1001	0.0711	0.001
C	0.04	1003	0.0711	0.001
D	0.05	1004	0.0712	0.001
E	0.1	1008	0.0713	0.001
F	0.5	1043	0.0728	0.0012

and mass transfer based on the theoretical studies on coalescence inhibition and mass transfer in contaminated solutions. The characteristics of different concentrations of a particular electrolyte are such that the physical properties are barely modified but are capable or modifying the hydrodynamics of the system by covering the contact area provided by the bubbles. Experimental solutions of $CaCl_2$ from a previous study by Ruzicka et al. [100] will be used, see Table 5.

According to Zahradník et al. [101] the critical concentration for the step decrease in bubble coalescence is 0.056 M for $CaCl_2$. Two solutions, E and F, over this concentration will also be simulated. Gas flow rates from 0.0075 to 0.035 m/s, within the homogeneous regime according to the experimental results by Ruzicka et al. [100], will be used.

According to Holtzapple et al. and Akita [102,104], the diffusion coefficients do not vary strongly with salt concentration but depend on the liquid viscosity. Since the addition of $CaCl_2$ did not modify the viscosity of the solution [20,100] for the range of salt concentrations used in this work, $[CaCl_2] < 0.5$ M, diffusivity was assumed to be

$$\frac{D_{salt}}{D_{water}} \approx 1 \tag{55}$$

Even considering the range of diffusion coefficients given by Hikita et al. [8], for the concentrations of the solutions employed in this work, the previous approximation is reasonable.

4. Comparison between calculated and modelled results

The model simulates, first, the dispersion of bubbles generated in the column and second, k_La, by combining the contact area given by the dispersion of bubbles and the liquid-film resistance of each bubble size in the vessel.

4.1. Effect of surface tension (and liquid density)

First we are going to evaluate the effect of the physical properties of the liquid and the ability of the model to simulate the Sauter-mean bubble diameter. It is assumed that the surfaces of the bubbles behave as free mobile.

Thus, in the framework of the model proposed before, Eq. (10) is used for computing the bubble rising velocity and Eq. (18) is implemented to calculate the liquid drainage time to reach the critical film thickness. The parameter in the population balance model is the critical Weber number. The starting point is $We_c = 5$, the value obtained for the air–water system [41]. We run the model for different virtual solutions in Table 4. The calculated values of d_{32} from the equation developed by Akita and Yoshida [88] Eq. (42) were used to verify the model.

Fig. 2 plots the comparison between the experimental Sauter-mean bubble diameter and the simulated one for the virtual solutions in Table 4 using $We_c = 5$ in all the cases. Good agreement is found which means that neither liquid density nor surface tension modifies the critical Weber number. Thus, in pure liquids, only liquid viscosity affects We_c. After this validation, the results showed by Pohorecki et al. [56] can also be explained. Pohorecki et al. [56] modelled bubble dispersions in organic liquids using constant We_c based on the fact that neither liquid density nor surface tension affects We_c.

Once we have checked the effect of the liquid density and surface tension on d_{32} for non-real solutions, a real fluid is evaluated. A typical pure liquid with visocosity close to that of water, cyclohexane [34], is used for a final validation of the model regarding the effect of surface tension and liquid density on the hydrodynamics and mass transfer. Using break-up and coalescence closures for pure liquids as before and assuming $We_c = 5$, the comparison between the values obtained using Eq. (42) and the modelled ones can be seen in Fig. 3, good results were obtained.

Once the bubble distribution is modelled, the mass transfer rates must be evaluated for a complete validation of the model. For solutions I to V and for cyclohexane, since mobile bubbles are assumed, k_L is that given by Higbie's theory, Eq. (44) only corrected due to the presence of more bubbles in the bubble column [41,97,98]. Figs. 4 and 5 show the comparison between the calculated k_La obtained using Eq. (52) and the calculated ones for the virtual solutions and for cyclohexane. In general, good agreement is found. The differences between the simulated and the experimental results are related to the ability of the model to predict the Sauter-mean bubble size and thus the contact area.

4.2. Effect of surfactants

4.2.1. Partially covered surfaces

The next step in modelling the effect of surface active species on the mass transfer rates is evaluating the effect that those species have on the bubble surface and its result on k_La. As it has been explained along the paper, these species concentrate themselves on the surface of the bubbles modifying the drainage of the liquid-

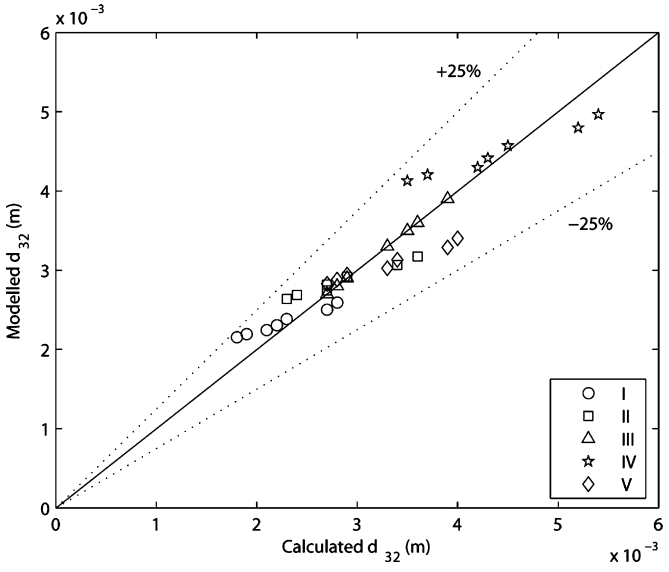

Fig. 2. Effect of physical properties to the Weber critical number.

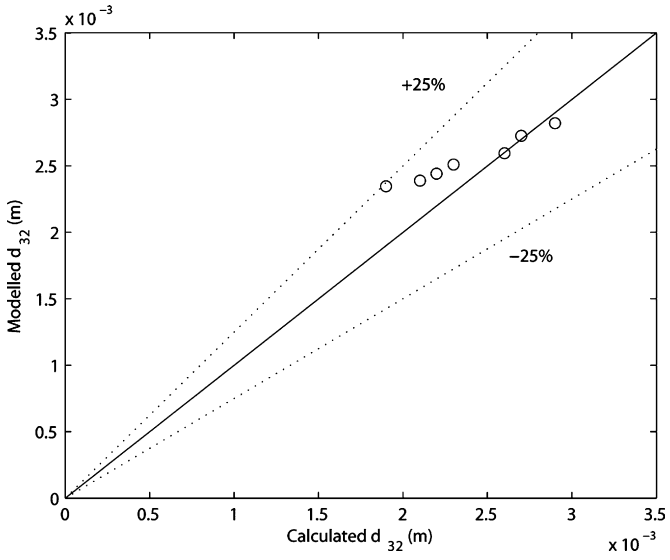

Fig. 3. Validation of the model with cyclohexane.

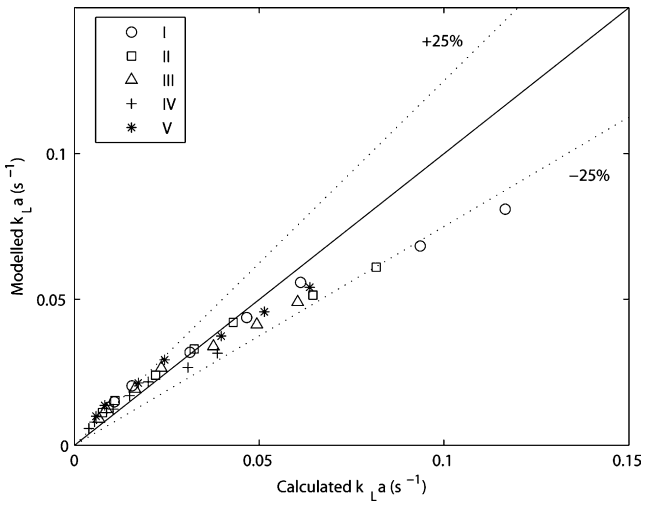

Fig. 4. Modelling mass transfer rates for virtual solutions.

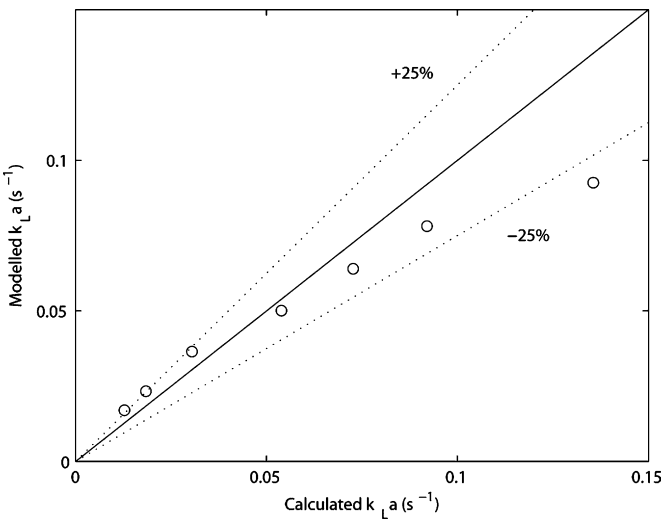

Fig. 5. Validation fo the model for cyclohexane.

Table 6
Properties of different solutions.

Solution	I (M)	We_c	Se
Air–water	0	5	0
A	0.03	3.5	0.4
B	0.06	2.5	0.6
C	0.12	2	0.8
D	0.15	1.5	0.9

films generated when two bubbles collide. Furthermore they affect the final breakage of the bubbles too.

Thus, for concentrations of $CaCl_2$ that are below the critical concentration that reduces drastically the coalescence, a partially mobile drainage model for bubble coalescence is implemented, Eq. (20). Another important consideration is the fact that bubble velocity gets reduced due to the presence of this species surrounding the bubbles. Thus, Eqs. (11)–(13) are used to implement this effect. Finally, we are going to use the Weber critial number as a parameter to evaluate the effect of the contaminated surface on bubble break-up.

In the case of the presence of electrolytes in solution, the main characteristic of the solutions is the ionic strengh since, as it can be seen in Table 6, no big change in the physical properties of the liquid is shown due to the presence of ions. Table 6 shows the values of We_c for different ionic forces. Using these values, good agreement can be seen between the experiemental Sauter-mean bubble sizes calcualted using Eqs. (42) and (43) and the modelled ones, Fig. 6.

If we plot the We_c versus the ionic stregth, I, see Fig. 7, a linear profile is found. Eq. (56) shows the correlation developed.

$$We_c = -21I + 4.4 \tag{56}$$

There is a linear relationship between the ionic strength and the critical Weber number. The modification of bubble contact area before its breakage changes the contaminant concentration on the surface and thus the properties of the film to be broken in the breakage of the bubble. The stretching of the surface together with the concentration and reallocation of the acumulated species on the surface of the bubble makes this film more unstable and breaks easier than in pure water.

Once the model matches the hydrodynamics, the simulation of the volumetric mass transfer coefficient is attempted. The increment in the concentration of salt increases the surface of the bubbles covered by contaminants. However, it is difficult to pre-

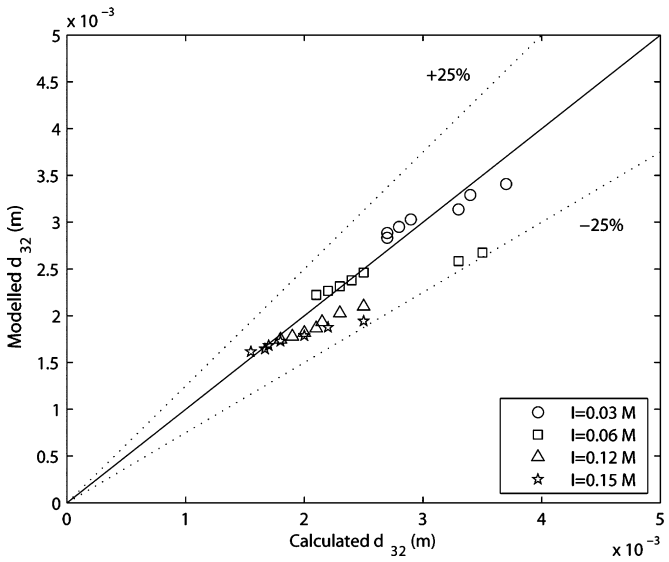

Fig. 6. Validation of the mean bubble size for partially covered bubble surfaces.

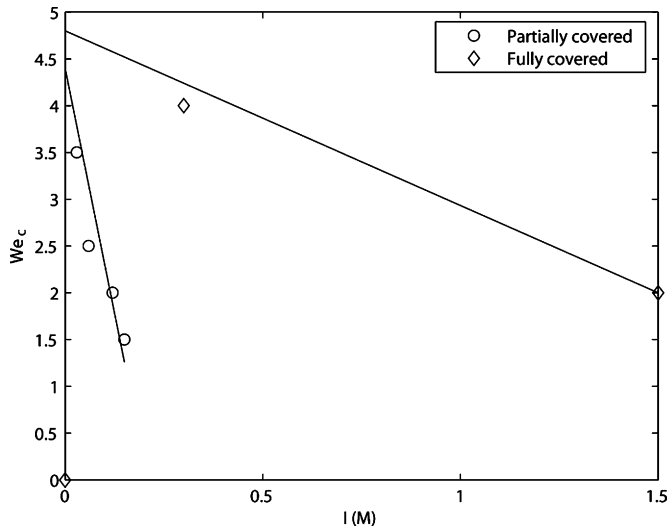

Fig. 7. Profile of the Weber critical number with ionc strenght and bubble surface behaviour.

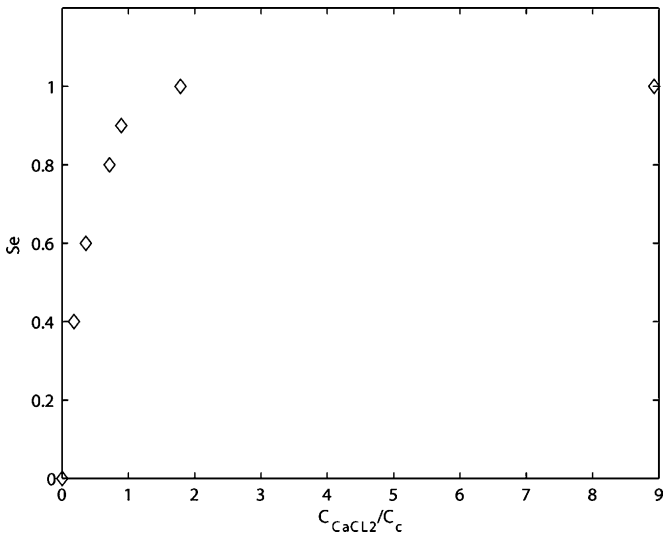

Fig. 9. Profile of surperficial area covered as fuction of the relative concentration of salt.

cisely determine the coverage ratio. In order to have an estimation we correlated the contact area generated by the bubbles and the surface coverage cosidering that the critical concentration 0.056 M represents $Se = 1$ meanwhile, $Se = 0$ is the air–water system. Table 6 shows approximate values of surface coverage that have been used to model $k_L a$. With these values of surface coverage, good agreement can be found between the values of $k_L a$ obtained using Hikita's equation (53) and the modelled ones, see Fig. 8. Fig. 9 shows the profile of surface coverage, *Se*, with the relative concentration of $CaCl_2$. As it is expected, it is not linear because the increment in contact area with the decrease in the mean bubble size is not linear either. Even assuming that *Se* is an adjustable parameter, only *Se* and We_c are the model parameters and both have a strong physical meaning.

4.2.2. Completely covered surfaces

If the concentration of salts exceeds the critical one, we may consider that the surface of the bubble is completely covered by surface active species, changing the behaviour of the surface. In order to avoid the fact that part of the bubble surface remains clean during bubble deformation as a result of an increase or modification of contact area, salt concentrations at least twice the critical one are used in this part of the study. The experimental solutions with this behaviour are solutions E and F in Table 5, from a previous study in the literature [100]. Bigger concentrations should not be used because the correction factor for the Sauter-mean bubble diameter in the experimental equation (42) and (43) ranges from 0 to 1 M. Even if solution F is already out of the range, we are going to assume that the correction can be used due to the asymptotic behaviour close to the upper concentration limit [90].

For salt concentrations over the critical one, the coalescence rates are dramatically reduced because the presence of contaminants surrounding the bubble reduces the mobility of the liquid-film that has to be drained before two colliding bubbles actually coalesce. To account for this effect the drainage time is calculated using Eq. (21). Again, the critical Weber number is the only parameter of the population balance.

Fig. 10 shows the comparison between the experimental Sauter-mean bubble diameter calculated using Eqs. (42) and (43), and the modelled one employing We_c as in Table 7. Good agreement is found. Going back to Fig. 7, it also showed the profile of the We_c ver-

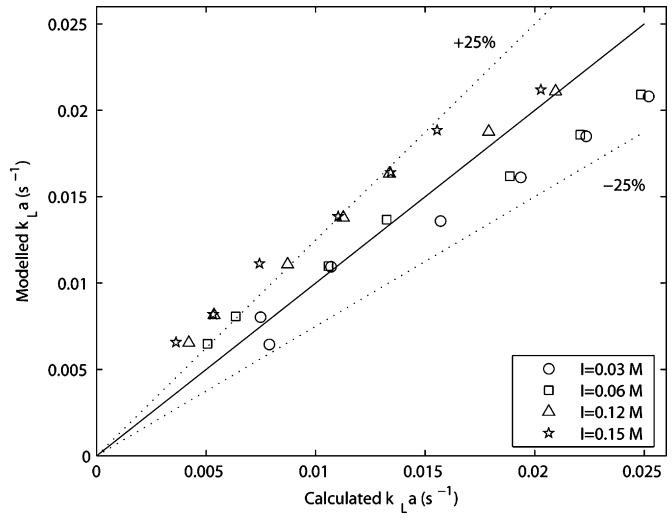

Fig. 8. Validation of the volumetric mass transfer coefficient for partially covered bubble surfaces.

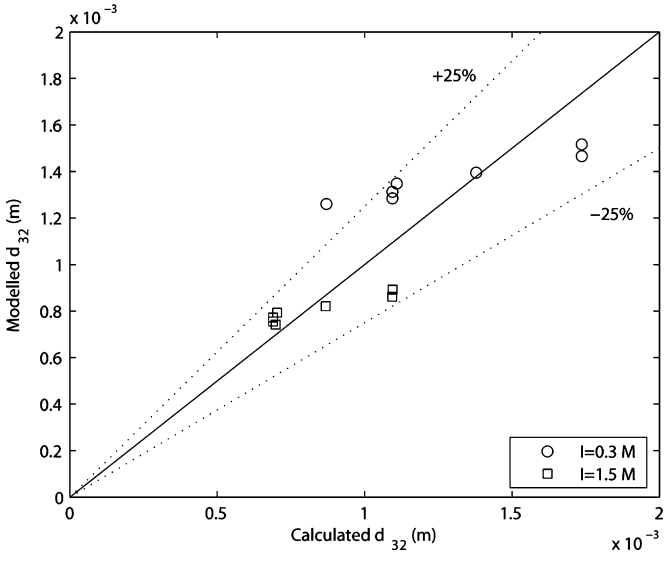

Fig. 10. Validation of the mean bubble size for fully covered bubble surfaces.

Table 7
Characteristics of solutions for immobile surfaces.

Solution	I (M)	We_c	Se
E	0.3	4	1
F	1.5	2	1

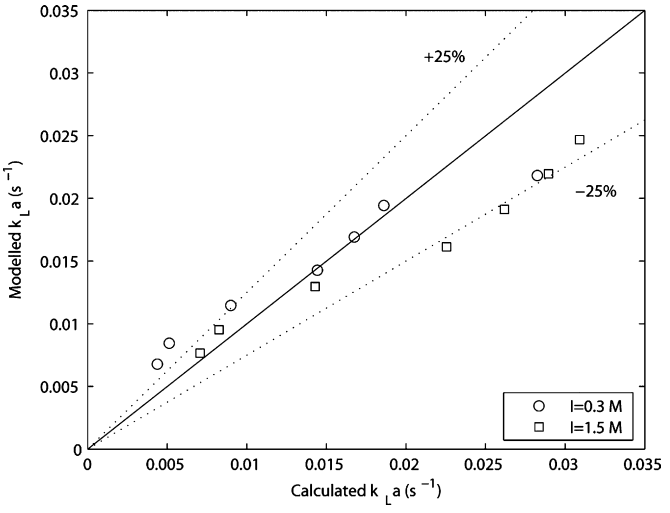

Fig. 11. Validation of the volumetric mass transfer coefficient for fully covered bubble surfaces.

sus the ionic strength for fully covered immobile surfaces. A linear profile is found but it is different than the one obtained for partially covered surfaces. There is a discontinuity in the We_c when the surfaces are partially or fully covered. It is expected that the bubble surfaces will behave differently because of the presence of surface active species provides new characteristics to the boundary layer around the bubbles and thus, their break-up is also different. For $I = 0$ We_c has been considered to be 5 since the effect of liquid properties does not affect it. Eq. (56) represents the profile for the critical Weber number in case of bubbles whose surface is immobile. For bigger concentrations of surface active species, bubble breakage becomes easier.

$$We_c = -1.9I + 4.8 \quad (57)$$

The liquid-film resistance, k_L, for immobile surfaces, $Se = 1$, is given by Eq. (45). Fig. 11 shows the comparison between the simulated results and the ones from Eq. (53) [8]. Reasonable good agreement is found. The better the hydrodynamics are modelled the more accurate the mass transfer coefficients are calculated, even taking into account the very limited number of adjustable parameters, in this case only the We_c.

5. Conclusions

Bubble column design is a key issue for the chemical and biochemical industries due to the wide range of application. So far, different adjustable parameters have been used to fit the experimental values of bubble diameters and $k_L a$ and the theoretical ones. The physical meaning of the theoretical parameters of the model allows a better understanding of the operation of bubble columns.

The theoretical closures for bubble calescence in presence of contaminants have been successfully implemented and allow reducing the parameters traditionally used for PBM to just the critical Weber number which at the same time gives information regarding the stability of the bubbles under different experimental conditions.

The critical Weber number turns out to be a function of the ionic strength because it is a measurement of the properties of the film that must be broken to divide a bubble into two. Further experimental effort must be made to identify if the size of the ions affects We_c or the ionic strength of a solution if the best parameter to characterize it.

The volumetric mass transfer coefficients are fairly well predicted as function of the bubble coverage taking into account that the theoretical equations for k_L must be corrected due to the fact that the bubbles do not travel alone and the concentration gradients are affected by the presence of other bubbles. The only parameter is the physical coverage of the bubbles, Se. However, different species may have different behaviour in terms of its effect on the surface of the bubble.

Further research on mass transfer in laboratory, pilot plant scale bubble columns must be performed to evaluate the effect of different salts in case the size of the ions affect bubble coalescence or breakage, alcohols and surfactants on contact area and volumetric mass transfer coefficient but a good framework to understand the behaviour of surface active species has been established with this work.

Acknowledgments

The support of the Ministerio de Educación y Ciencia of Spain and the Fulbright commission providing a MICINN-Fulbright fellowship to M. Martín is greatly acknowledge. The authors also acknowledge the funds by project CTQ2008-04727.

Appendix A. Supplementary data

Supplementary data associated with this article can be found, in the online version, at doi:10.1016/j.cej.2009.08.009.

References

[1] Y.T. Shah, B.G. Kelkar, S.P. Godbole, W.D. Deckwert, Design parameters estimations for bubble column reactor, AIChE J. 28 (1982) 353–379.
[2] N. Kantarci, F. Borak, K.O. Ulgen, Bubble column reactor, Proc. Biochem. 40 (2005) 2263–2283.
[3] H.A. Jakobsen, H. Lindborg, C.A. Dorao, Modeling of bubble column reactors: progress and limitations, Ind. Eng. Chem. Res. 44 (2005) 5107–5151.
[4] P.F. Davis, A. Remuzzi, E.J. Gordon, C.F. Dewey, M.A. Gimbrone Jr., Turbulent fluid shear stresses induces vascular endothelial cell turnover in vitro, Proc. Natl. Acad. Sci. U.S.A. 83 (1986) 2114–2117.
[5] J. Hua, L.E. Erickson, T.Y. Yiin, L.A. Glasgow, A review of the effects of shear and interfacial phenomena on cell viability, Crit. Rev. Biotechnol. 13 (1993) 305–328.
[6] F. Garcia-Ochoa, E. Gomez, Bioreactor scale-up and oxygen transfer rate in microbial processes: an overview, Biotech. Adv. 27 (2009) 153–176.
[7] K. Akita, F. Yoshida, Bubble size, interfacial area, and liquid phase mass transfer coefficients in bubble columns, Ind. Eng. Chem. Proc. Des. Dev. 13 (1974) 84–91.
[8] H. Hikita, S. Asai, K. Tanigawa, K. Segawa, M. Kitao, The volumetric liquid-phase mass transfer coefficient in bubble columns, Chem. Eng. J. 22 (1981) 61–69.
[9] Y. Kawase, B. Halard, M. Moo-Young, Theoretical prediction of volumetric mass transfer coefficients in bubble columns for Newtonian and non-Newtonian fluids, Chem. Eng. Sci. 42 (1987) 1609–1617.
[10] K. Shimizu, S. Takada, K. Minekawa, Y. Kawase, Phenomenological model for bubble column reactors: prediction of gas hold-ups and volumetric mass transfer coefficients, Chem. Eng. J. 78 (2000) 21–28.
[11] T. Wang, J. Wang, Numerical simulations of gas–liquid mass transfer in bubble columns with a CFD-PBM coupled model, Chem. Eng. Sci. 62 (2007) 7107–7118.
[12] K.J. Myers, M.P. Duduković, P. Ramachandran, A. Modeling, Liquid phase chemical reaction and interphase mass transfer in churn turbulent bubble columns, Chem. Eng. Sci. 42 (1987) 2757–2766.
[13] R. Krishna, J.M. van Baten, Mass transfer in bubble columns, Catal. Today (2003) 79–80.
[14] Lu Han, H.Al-Dahhan Muthanna, Gas–liquid mass transfer in a high pressure bubble column reactor with different sparger designs, Chem. Eng. Sci. 62 (2007) 131–139.
[15] H. Dhaouadi, S. Poncin, J.M. Hornut, N. Midoux, Gas–liquid mass transfer in bubble column reactor: analytical solution and experimental confirmation, Chem. Eng. Process. 47 (2008) 548–556.

[16] R. Lemoine, A. Behkish, L. Sehabiague, Y.J. Heintz, R. Oukaci, B.I. Morsi, An algorithm for predicting the hydrodynamic and mass transfer parameters in bubble column an slurry bubble column reactors, Fuel Process. Tech. 89 (2008) 322–343.
[17] H. Funahashi, K.I. Hirai, T. Yoshida, H. Taguchi, Mechanistic analysis of xanthan gum production in a stirred tank, J. Ferment. Technol. 66 (1988) 355–364.
[18] E. Deziel, G. Paquette, R. Villemur, F. Lepine, J. Bisaillon, Biosurfactant production by a soil pseudomonas strain growing on polycyclic aromatic hydrocarbons, Appl. Environ. Microbiol. 62 (1996) 1908–1912.
[19] F.J. Montes, J. Catalán, M.A. Galán, Measurement of k_La in yeast broths, Proc. Biochem. 34 (1999) 549–555.
[20] L.-K. Ju, S.H. Chester, R.F. Baddour, Simultaneous measurements of oxygen diffusion coefficients and solubilities in fermentation media with polarographic oxygen electrodes, Biotech. Bioeng. 31 (1988) 995–1005.
[21] K.G. Clarke, L.D.C. Correia, Oxygen transfer in hydrocarbon-aqueous dispersions and its applicability to alkane bioprocesses: a review, Biochem. Eng. J. 39 (2008) 405–429.
[22] M. Martín, F.J. Montes, M.A. Galán, Mass transfer rates from oscillating bubbles in bubble columns operating with viscous fluids, Ind. Eng. Chem. Res. 47 (2008) 9527–9536.
[23] L. Rodrigues, J. Teixeira, R. Oliveira, H.C. van der Mei, Response surface optimization of the medium components for the production of biosurfactants by probiotic bacteria, Proc. Biochem. 41 (2006) 1–10.
[24] V. Linek, T. Moucha, J. Sinkule, Gas–liquid mass transfer in vessels stirred with multiple impellers—I. Gas–liquid mass transfer characteristics in individual stages, Chem. Eng. Sci. 51 (1996) 3203–3212.
[25] V. Linek, T. Moucha, J. Sinkule, Gas–liquid mass transfer in vessels stirred with multiple impellers—II. Modelling of gas–liquid mass transfer, Chem. Eng. Sci. 51 (1996) 3875–3879.
[26] G. Vázquez, M.A. Cancela, C. Riverol, E. Alvarez, J.M. Navaza, Application of the Danckwerts method in a bubble column. Effects of surfactants on mass transfer coefficient and interfacial area, Chem. Eng. J. 78 (2000) 13–19.
[27] M. Bouaifi, G. Hebrard, D. Bastoul, M. Roustan, An analogic study about gas hold-up, bubble size. Interfacial area and mass transfer coefficients in agitated gas–liquid reactors and bubble columns, Chem. Eng. Process. 40 (2001) 97–111.
[28] S.S. Alves, C.I. Maia, J.M.T. Vasconcelos, A.J. Serralheiro, Bubble size in aerated stirred tanks, Chem. Eng. J. 89 (2002) 109–117.
[29] J.M.T. Vasconcelos, S.P. Orvalho, S.S. Alves, Gas–liquid mass transfer to single bubbles: effect of surface contamination, AIChE J. 48 (2002) 1145–1154.
[30] J.M.T. Vasconcelos, J.M.L. Rodrigues, S.C.P. Orvalho, S.S. Alves, R.L. Mendes, A. Reis, Effect of contaminants on mass transfer coefficients in bubble column and airlift contactors, Chem. Eng. Sci. 58 (2003) 1431–1440.
[31] P. Painmanakul, K. Loubière, G. Hébrard, M. Mietton-Peuchot, M. Roustan, Effect of surfactants on liquid-side mass transfer coefficients, Chem. Eng. Sci. 60 (2005) 6480–6491.
[32] V. Linek, M. Moucha, M. Kordac, Mechanism of mass transfer from bubbles in dispersions: part I. Danckwerts' plot method with sulphite solutions in the presence of viscosity and surface tension changing agents, Chem. Eng. Process. 44 (2005) 353–361.
[33] V. Linek, M. Kordac, T. Moucha, Mechanism of mass transfer from bubbles in dispersions: part II. Mass transfer coefficients in stirred gas–liquid reactor and bubble column, Chem. Eng. Process. 44 (2005) 121–130.
[34] H. Chaumat, A.M. Billet, H. Delmas, Hydrodynamics and mass transfer in bubble column: influence of liquid phase surface tension, Chem. Eng. Sci. 62 (2007) 7378–7390.
[35] P. Painmanakul, G. Hébrard, Effect of different contaminants on the α-factor: local experimental method and modeling, Chem. Eng. Res. Des. 86 (2008) 1207–1215.
[36] D. Gómez-Díaz, J.M. Navaza, B. Sanjurjo, Mass-transfer enhancement or reduction by surfactant presence at a gas–liquid interface, Ind. Eng. Chem. Res. 48 (2009) 2671–2677.
[37] S.S. Alves, C.I. Maia, J.M.T. Vasconcelos, Gas–liquid mass transfer coefficient in stirred tanks interpreted through bubble contamination kinetics, Chem. Eng. Proc. 43 (2004) 823–830.
[38] V. Linek, M. Kordac, M. Fujasova, T. Moucha, Gas–liquid mass transfer coefficient in stirred tanks interpreted through models of idealized eddy structure of turbulence in the bubble vicinity, Chem. Eng. Process. 43 (2004) 1511–1517.
[39] P. Moilanen, M. Laakkonen, O. Visuri, J. Aittamaa, Modeling local gas–liquid mass transfer in agitated viscous shear-thinning dispersions with CFD, Ind. Eng. Chem. Res. 46 (2007) 7289–7299.
[40] A. Gäbler, M. Wegener, A.R. Paschedag, M. Kraume, The effect of pH on experimental and simulation results of transient drop size distributions in stirred liquid–liquid dispersions, Chem. Eng. Sci. 61 (2006) 3018–3024.
[41] M. Martín, F.J. Montes, M.A. Galán, Mass transfer from oscillating bubbles in bubble columns, Chem. Eng. J. 151 (2009) 79–88.
[42] J.E. Botello-Álvarez, J.L. Navarrete-Bolaños, H. Hugo Jiménez-Islas, A. Estrada-Baltazar, R. Rico-Martínez, Improving mass transfer coefficient prediction in bubbling columns via sphericity measurements, Ind. Eng. Chem. Res. 43 (2004) 6527–6533.
[43] S. Nedeltchev, U. Jordan, A. Schumpe, Correction of the penetration theory based on mass-transfer data from bubble columns operated in the homogeneous regime under high pressure, Chem. Eng. Sci. 62 (2007) 6263–6273.
[44] J.J. Jeng, J.R. Maa, Y.M. Yang, Surface effects and mass transfer in bubble column, Ind. Eng. Chem. Proc. Des. Dev. 25 (1986) 974–978.
[45] M.J. Prince, H.W. Blanch, Bubble coalescence and break-up in air sparged bubble columns, AIChE J. 36 (1990) 1485–1499.
[46] A.K. Chesters, The modeling of coalescence processes in fluid-liquid dispersion: a review of current understanding, Trans. Inst. Chem. Eng. 69 (1991) 259–270.
[47] M. Simon, Koaleszenz von Tropfen und Tropfenschwärmen, Ph.D. thesis, Technischen Universität Kaiserslautern, 2004.
[48] R.K. Sinnot, Coulson & Richardson Chemical Engineering, vol. 6: An Introduction to Chemical Engineering Design, 3rd ed., Butterworth Heinemann, Oxford, 1999.
[49] D.N. Miller, Scale up of agitated vessels gas liquid mass transfer, AIChE J. 20 (1974) 445–453.
[50] M.C. Weinberg, Surface tension effects in gas bubble dissolution and growth, Chem. Eng. Sci. 36 (1981) 137–141.
[51] M. Martín, F.J. Montes, M.A. Galán, On the influence of liquid properties on bubble volume and generation times, Chem. Eng. Sci. 61 (2006) 5196–5203.
[52] E.E. Ludwig, Applied Process Design for Chemical and Petrochemical Plants, vol. 2, Gulf Publishing Company, Houston, 1964.
[53] J.F. Walter, H.W. Blanch, Bubble break-up in gas–liquid bioreactors: break-up in turbulent flow, Chem. Eng. J.: Biochem. Eng. J. 32 (1986) b7–b17.
[54] R.P. Hesketh, A.W. Etchells, T.W. Russel, Bubble breakage in pipeline, Chem. Eng. Sci. 46 (1991) 1–9.
[55] P.M. Wilkinson, A.V. Schayk, J.P.M. Spronken, L.L.V. Dierendonk, The influence of gas density and liquid properties on bubble breakup, Chem. Eng. Sci. 48 (1993) 1213–1226.
[56] R. Pohorecki, W. Moniuk, P. Bielski, A. Zdrójkowski, Modelling of the coalescence/redispersion processes in bubble columns, Chem. Eng. Sci. 56 (2001) 6157–6164.
[57] M. Martín, F.J. Montes, M.A. Galán, Influence of impeller type on the bubble break-up process in stirred tanks the effect of the impeller geometry on the break-up of bubbles, Ind. Eng. Chem. Res. 47 (2008) 6251–6263.
[58] M. Martín, F.J. Montes, M.A. Galán, Bubble coalescence at sieve plates: II. Effect of coalescence on mass transfer. Superficial area versus bubble oscillations, Chem. Eng. Sci. 62 (2007) 1741–1752.
[59] R.V. Chaudhari, H. Hofmann, Coalescence of gas bubbles in liquids, Revs. Chem. Eng. 10 (1994) 131–190.
[60] V.S.J. Craig, Bubble coalescence and specific-ion effects, Curr. Opin. Colloid Interface Sci. 9 (2004) 178–184.
[61] G. Marrucci, A theory of coalescence, Chem. Eng. Sci. 24 (1969) 975–985.
[62] T.D. Hodgson, D.R. Woods, The effect of surfactants on the coalescence of a drop at an interface, J. Colloid Interface Sci. 30 (1969) 429–446.
[63] J.-D. Chen, P.S. Hahn, J.C. Slattery, Coalescence time for a small drop or bubble at a fluid–fluid interface, AIChE J. 30 (1984) 622–630.
[64] T.O. Oolman, H.W. Blanch, Bubble coalescence in stagnant liquids, Chem. Eng. Commun. 43 (1986) 237–261.
[65] C.-H. Lee, L.E. Erickson, L.A. Glasgow, Bubble break-up and coalescence in turbulent gas–liquid dispersions, Chem. Eng. Commun. 59 (1987) 65–84.
[66] D. Li, S. Liu, Coalescence between small bubbles or drops in pure liquids, Langmuir 12 (1996) 5216–5220.
[67] F. Lehr, M. Milies, D. Mewes, Bubble-size distributions and flow fields in bubble columns, AIChE J. 48 (2002) 2426–2443.
[68] C.P. Ribeiro Jr., D. Mewes, On the effect of liquid temperature upon bubble coalescence, Chem. Eng. Sci. 61 (2006) 5704–5716.
[69] C.P. Ribeiro Jr., D. Mewes, The effect of electrolytes on the critical velocity for bubble coalescence, Chem. Eng. J. 126 (2007) 23–33.
[70] M. Martín, J.M. García, F.J. Montes, M.A. Galán, On the effect of sieve plate configuration on the coalescence of bubbles, Chem. Eng. Process. 47 (2008) 1799–1809.
[71] G. Drogaris, P. Weiland, Studies of coalescence of bubble pairs, Chem. Eng. Commun. 23 (1983) 11–26.
[72] R.R. Lessard, S.A. Zieminski, Bubble coalescence and gas transfer in aqueous electrolytic solutions, Ind. Eng. Chem. Fund. 10 (1971) 260–269.
[73] G. Marrucci, L. Nicodemo, Coalescence of gas bubbles in aqueous solutions of inorganic electrolytes, Chem. Eng. Sci. 22 (1967) 1257–1265.
[74] M.J. Prince, H.W. Blanch, Transition electrolyte concentrations for bubble coalescence, AIChE J. 36 (1990) 1425–1429.
[75] J.C. Rotta, Turbulence Stromungen, B.G. Teubner, Stuttgart, 1972.
[76] R.M. Griffith, The effect of surfactants on the terminal velocity of drops and bubbles, Chem. Eng. Sci. 17 (1962) 1057–1070.
[77] R. Clift, J.R. Grace, M.E. Weber, Bubbles Drops and Particles, Academic press, New York, 1978.
[78] M. Jamialahmadi, H. Miiller-Steinhagen, Effect of alcohol, organic acid and potassium chloride concentration bubble size, bubble rise velocity and gas hold-up in bubble columns, Chem. Eng. J. 50 (1992) 47–56.
[79] S.S. Alves, J.M.T. Vasconcelos, S.P. Orvalho, Effect of bubble contamination on rise velocity and mass transfer, Chem. Eng. Sci. 60 (2005) 1–9.
[80] J.R. Grace, T. Wairegi, T.H. Nguyen, Shapes and velocities of single drops and bubbles moving freely through immiscible liquids, Trans. Inst. Chem. Eng. 54 (1976) 167–173.
[81] S.K. Friedlander, Smoke, Dust and Haze, Wiley, New York, 1977.
[82] C.A. Coulaloglou, L.L. Tavlarides, Description of interaction processes in agitated liquid–liquid dispersions, Chem. Eng. Sci. 32 (1977) 1289–1297.
[83] G. Marrucci, L. Nicodemo, D. Acierno, Bubble coalescence under controlled conditions, Proc. Inter. Symp. Res. Conc. Gas–Liquid Flow (1969) 95–108.
[84] J.O. Hinze, Fundamentals of the hydrodynamic: mechanism of slitting in dispersion processes, AIChE J. 1 (1955) 1289–1295.

[85] F. Risso, J. Fabre, Oscillations and break-up of a bubble immersed in a turbulent field, J. Fluid Mech. 372 (1998) 323–355.
[86] C. Fleischer, S. Becker, G. Eigenberger, Detailed modeling of the chemisorption of CO_2 into NAOH in a bubble column, Chem. Eng. Sci. 51 (1996) 1715–1724.
[87] A. Kulkarni, Y.T. Shah, B.G. Kelkar, Gas holdup in bubble column with surface-active agents: a theoretical model, AIChE J. 33 (1987) 690–693.
[88] K. Akita, F. Yoshida, Gas hold-up and volumetric mass transfer coefficient in bubble columns, Ind. Eng. Chem. Proc. Des. Dev. 12 (1973) 76–80.
[89] H. Hikita, S. Asai, K. Tanigawa, K. Segawa, M. Kitao, Gas hold-up in bubble columns, Chem. Eng. J. 20 (1980) 59–67.
[90] S.A. Zieminski, R.C. Whittemore, Behavior of gas bubbles in aqueous electrolyte solutions, Chem. Eng. Sci. 26 (1971) 509–520.
[91] G. Keitel, U. Onken, Inhibition of bubble coalescence by solutes in air/water dispersions, Chem. Eng. Sci. 37 (1982) 1635–1638.
[92] D. Ruen-ngam, P. Wongsuchoto, A. Limpanuphap, T. Charinpanitkul, P. Pavasant, Influence of salinity on bubble size distribution and gas–liquid mass transfer in airlift contactors, Chem. Eng. J. 141 (2008) 222–232.
[93] E. Sada, H. Kumazawa, C.-H. Lee, H. Narukawa, Gas–liquid interfacial area and liquid-side mass-transfer coefficient in a slurry bubble column, Ind. Eng. Chem. Res. 26 (1987) 112–116.
[94] R. Higbie, The rate of absorption of a pure gas into a still liquid during a short time of exposure, Trans. IChemE 31 (1935) 365–389.
[95] N. Frossling, UJ bber die verduJnstung fallenden tropfen (evaporation off alling drops), Gerlands Beitage zur Geophysik 52 (1938) 170–216.
[96] R. Sardeing, P. Painmanakul, G. Hébrard, Effect of surfactants on liquid-side mass transfer coefficients in gas–liquid systems: a first step to modeling, Chem. Eng. Sci. 61 (2006) 6249–6260.
[97] A. Koynov, J.G. Khinast, G. Tryggvason, Mass transfer and chemical reactions in bubble swarms with dynamic interfaces, AIChE J. 51 (2005) 2786–2800.
[98] J.C. Lamont, D.S. Scott, An eddy cell model of mass transfer into surface of a turbulent liquid, AIChE J. 16 (1970) 513–519.
[99] A.A. Kulkarni, J.B. Joshi, V.R. Kumar, B.D. Kulkarni, Simultaneous measurement of hold-up profiles and interfacial area using LDA in bubble columns: predictions by multiresolution analysis and comparison with experiments, Chem. Eng. Sci. 56 (2001) 6437–6445.
[100] M.C. Ruzicka, M.M. Vecer, S. Orvalho, J. Drahoš, Effect of surfactant on homogeneous regime stability in bubble column, Chem. Eng. Sci. 63 (2008) 951–967.
[101] J. Zahradník, M. Fialová, V. Linek, The effect of surface-active additives on bubble coalescence in aqueous media, Chem. Eng. Sci. 54 (1999) 4757–4766.
[102] M.T. Holtzapple, P.T. Eubank, M.A. Matthews, A comparison of three models for the diffusion of oxygen in electrolyte solutions, Biotech. Bioeng. 34 (1989) 964–970.
[103] W.D. Deckwer, On the mechanism of heat transfer in bubble column reactors, Chem. Eng. Sci. 35 (1980) 1341–1346.
[104] K. Akita, Diffusivities of gases in aqueous electrolyte solutions, Ind. Eng. Chem. Fundam. 20 (1981) 89–94.